Journal of
Computational and Theoretical Nanoscience
Vol. 3, 670–683, 2006

Mechanics of Protein Crystals: Atomistic Modeling of Elasticity and Fracture

Markus J. Buehler

Department of Civil and Environmental Engineering, Massachusetts Institute of Technology, Cambridge, MA 02139, USA

The structure, behavior, and mechanical properties of proteins plays an overarching role in biological systems. In recent years, materials based on proteins have also been proposed as a basis of new materials for medical and technological applications. In this article, we report classical molecular dynamics modeling of the elasticity and fracture behavior of protein crystals. We consider two proteins, a small protein α-conotoxin PnIB from *conus pennaceus* and lysozyme, a well-studied enzyme that catalyzes breaking of glycosidic bonds. We calculate pressure–strain curves for different loading conditions, including uniaxial strain in three crystallographic directions and equitriaxial loading. Our modeling yields insight into the deformation mechanisms inside the protein molecules. We find that changes in internal displacements of backbone C_α-atoms, referred to as characteristic deformation profiles, can be linked with the macroscopic elastic response of the protein crystal. We demonstrate that simple sequence mutations may have a strong impact on elastic properties, indicating the potential of using amino acid mutations to tailor mechanical properties. We observe that such sequence mutations induce changes in the characteristic displacement profiles, which lead to modified elastic response. We also report a study of mode I fracture of protein crystals, showing some molecular details of dynamical crack propagation in protein crystals.

Keywords: Mechanics, Protein Crystals, Elasticity, Fracture, Deformation, Molecular Modeling, Biology, Enzyme, Force Field.

RESEARCH ARTICLE

1. INTRODUCTION

Biological materials and those inspired by Nature may be essential to face technological challenges related to new medical applications or novel concepts in sensor and actuator design that can be used to improve the reliability and robustness of devices.[1–5] Other applications are related to conservation of resources and development of novel environmentally benign structural or adhesion materials.[6–10]

The combination of
(i) high-level structural control of matter as achieved in nanoscience and nanotechnology, and
(ii) integration of living with non-living systems into novel technologies could play a critical role.[7, 8, 11–16]

Such approaches may also impact our molecular and cellular level understanding of how diseases develop and spread.[17, 18]

With increasing complexity, materials start to resemble systems or machines, so that the borderlines between the conventional concepts such as "machine" and "material" start to disappear. Integrating increased functionality into materials is a concept that has been used systematically by Nature for millions of years, and their exploitation for technological applications holds great promises, opening a new sub domain in materials research. Detailed and fundamental understanding of the properties of biological materials—beyond an empirical approach, using rigorous engineering principles—could play an essential role to enable design of such devices.[2, 16, 19]

Significant breakthroughs at the interfaces of materials science and biology have been achieved in the past decade. For example, genetically engineered biopolymers based on recombinant DNA technologies have been developed by Tirrell and coworkers.[13, 14] Those techniques represent attempts of translating nature's structural concepts into engineered materials. In principle, this requires an extremely high level of control of macromolecular architecture, far beyond conventional polymerization process. Tirrell and coworkers[13, 14] use protein engineering to genetically encode protein-based materials with desired features, and use biological systems for production of materials. Figure 1 illustrates this approach.

Among the variety of biological materials, those based on proteins hold particular promise because of their great flexibility in usage and their applications. For example, proteins play a critical role in developing Nature's finest

1546-198X/2006/3/670/014 doi:10.1166/jctn.2006.007

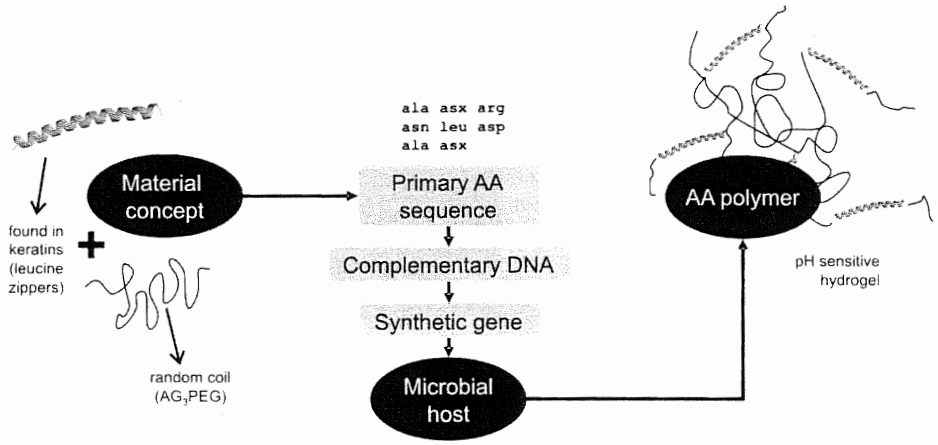

Fig. 1. Schematic viewgraph demonstrating the concept of recombinant DNA engineering to create artificial protein-based materials (amino acid (AA) polymers).[12–15, 48] Such novel material synthesis techniques provide unparalleled, extremely high level of control over the material microstructure, by combining the features of different proteins. The long-term goal of our modeling is to provide theoretical understanding of the mechanical behavior of those materials, suggesting systematic design improvements and models of the physics of deformation.

multi-functional, and nanostructured hierarchical materials, including bone, muscles, and tendon. Further, proteins are the basis of living materials and therefore are critical in understanding the interfaces of biology and materials technology. A wide range of diseases originate from molecular scale amino acid sequence mutations in proteins, leading to protein malfunction and spreading of the disease. Proteins also serve as growth factors in tissue growth, and play a critical role at the interfaces of cells with substrate materials or other cells, in particular under mechanical stimulation.

This wide-ranging utilization of proteins in Nature's design indicates immense opportunities for using them in new technologies. However, such developments are currently limited since the molecular scale understanding of many biological processes is still in its early stages. In particular, rigorous links between the properties of individual molecules and the complex phenomena arising from the interaction of thousands or millions of molecules represents an unresolved problem. The key to achieve full technological exploitation is to develop a sound scientific understanding of such molecular and atomistic mechanisms of the structure-function relationship of biological systems and materials.

In particular, the mechanical properties of many protein materials are still poorly understood, and little is known about their atomistic or molecular deformation mechanisms, and influence of the nanostructured design on the mechanical properties. Thus, our goal is to develop theoretical understanding of the relationships between small scale (e.g., primary structure) and macroscale (e.g., protein crystals), as visualized in Figure 2.

Among protein-based materials, crystals of proteins (in the remainder of this article referred to as "protein crystals") can be considered as one of the more simple classes of protein-based materials, since their structure can often be obtained from X-ray diffraction experiments with Ångstrom scale accuracy.

To advance the fundamental understanding of the mechanics of protein based materials, we carry out atomistic studies of the mechanical properties of protein crystals focusing on elasticity, plasticity, and fracture behavior. Even though protein crystals are not commonly used as structural or functional material, an improved understanding of their deformation mechanics may help to guide research in the area of other protein based materials. Protein crystals also play a role in certain diseases, such as sickle cell anemia, where hemoglobin molecules polymerize and form crystals when the oxygen concentration is lowered.[20] The mechanical stability of these crystals may be important for the progression of the disease.

1.1. Motivation to Study Mechanical Properties

The mechanical properties of materials are critical, even if the ultimate application of a material is not primarily related to its mechanical strength. Knowledge of the elastic moduli (i.e., how much a material stretches due an applied force), fracture strength (i.e., critical applied load when the material ruptures or bends), and adhesion properties (i.e., how strong two materials bind together) may become important during manufacturing processes or to ensure mechanical stability during operation of a device.

The ultimate strength of materials is dominated by the material behavior under presence of flaws such as cracks, vacancies, or other defects at the molecular level. Most materials have small defects embedded randomly within the material. Defects typically represent locations with large local stress, much larger than the applied stress. These locally large stresses lead to large forces between

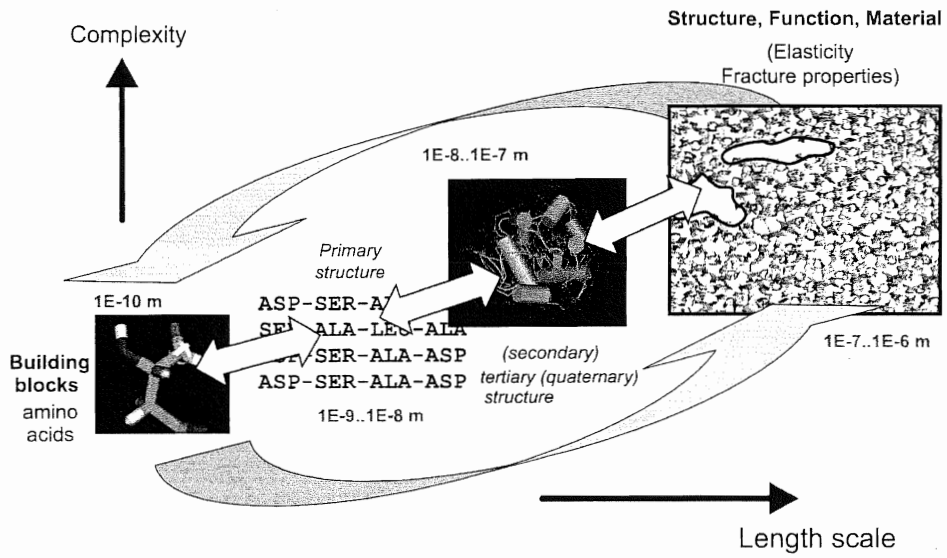

Fig. 2. Introduction and motivation for our studies. Our objective is to developing an understanding of the macroscopic properties of protein based materials ranging from the atomic scale up to the continuum scale where materials are employed in biological or structural applications. Proteins consist of different structural levels of detail, including the level of amino acid sequence (primary structure), arrangement of structural motifs, the overall folded three-dimensional geometry (tertiary structure), as well as the assembly of various proteins and/or substrates into agglomerates (quaternary structure).

atoms that may induce permanent breaking of atomic bonds or changes in the three-dimensional protein structure. To understand how strong a material is, it is critical to understand the nucleation and propagation properties of cracks. This motivates our studies of crack behavior in protein crystals.

1.2. Outline of this Paper

The plan of this paper is as follows. We start with a discussion of the computational method, briefly introducing classical force fields used to model the chemical bonds within the protein crystal. We then report studies of the elastic properties and large-strain deformation of a model system of a small protein α-conotoxin PnIB from *conus pennaceus*, deposited in the Protein Data Bank (PDB) with label PnIB 1AKG. In the following, we refer to this protein as "PnIB 1AKG." We also discuss studies of systematic mutations of individual amino acids used to alter the overall macroscopic elastic–plastic properties. Using a new concept of characteristic deformation profiles, we relate microscopic changes in displacements to the elastic properties. Moreover, we report studies of crack initiation and propagation in a crystal of PnIB 1AKG. We conclude the paper with studies of elasticity of lysozyme (deposited in the PDB with ID 194L, in the following referred to as "lysozyme 194L"). In addition to the calculation of pressure–strain curves for different loading conditions, we focus on the internal mechanisms associated with elasticity by studying the displacements of the C_α-atoms during deformation.

2. COMPUTATIONAL PROCEDURE AND ELASTICITY ANALYSIS

2.1. Interatomic Potential and Force Fields

Proteins constitute complex systems in which chemical bonds of different nature and strength interplay, including primary covalent and ionic bonds (strongest), hydrogen-bonds and van der Waals (vdW) interactions (weakest). It is not yet feasible to use quantum mechanical (QM) based descriptions[21,22] or first principles based reactive force fields (e.g., ReaxFF)[23] to describe these chemical bonds in systems that often comprise of several tens of thousands of atoms.

Here we use classical molecular dynamics (MD) with empirical interatomic potentials to model these interactions. Similar approaches are widely used to describe the properties of proteins.[24–31] Such potentials enable studies of systems containing 100,000 atoms and more. Such system sizes are critical in the study of fracture mechanics of protein crystals to enable representation of inhomogeneous stress and deformation fields that can span across tens of nanometers and larger.

Here we model the atomic interactions using the AMBER force field,[29] a widely used model for the atomic interactions in proteins.

2.2. Construction of Unit Cells from PDB Data

We build the crystal unit cells according to X-ray diffraction data obtained by experiment. These structures with atomic coordinates are taken directly from the PDB.

The charges of each atom are assigned according to the AMBER rules implemented in the tLEaP program (tLEaP is a program that generates input files for the AMBER program, consisting of structure and topology files describing the geometry, bond connectivity, and force field parameters). Hydrogen atoms are not resolved in the structure deposited in the PDB, and are added according to pH 7 using the tLEaP program. The protonation states of individual amino acids are also assigned according to pH 7 using the tLEaP program. The AMBER structure and topology files are then used to perform NAMD calculations.[28] We include only crystallographic water in the simulations to keep the computational effort low.

The energy of unit cells built based on the information deposited in the protein data base is minimized using the NAMD energy minimizing scheme before loading calculations are performed.

2.3. Computational Procedure for Elastic Properties

The calculations of the elastic and plastic response of perfect crystals are carried out with a single unit cell and periodic boundary conditions (PBCs), allowing to represent an infinite medium of protein crystal.

We strain the cell and the coordinates of each atom in the cell gradually in discrete steps $\Delta\varepsilon_{ij}$, assuming a homogeneous strain field as a first guess. While we displace all atoms in the unit cell according to the prescribed homogeneous strain field, we also modify the cell sizes L_x, L_y, and L_z accordingly. The method of straining the unit cell according to a specific strain tensor ε_{ij} is schematically depicted in Figure 3. The magnitude of strain increments $\Delta\varepsilon_{ij}$ varies between 0.25% to 1%.

We consider two loading cases. The first loading case is uniaxial tensile strain so that $i = j$ and thus the deformation state is described by the strain tensor ε_{ii}, where $i = 1, 2$, or 3, leading to only one nonzero component of ε_{ij}. The second loading case is equitriaxial or hydrostatic strain. Then, loading is applied simultaneously in three directions, thus ε_{ii} and $i = 1, 2, 3$, leading to three nonzero components of ε_{ij}.

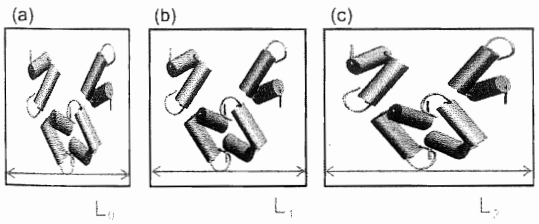

Fig. 3. Schematic demonstrating how uniaxial strain is applied to the unit cell. The unit cell is systematically strained, so that $L_1 = (1+\varepsilon_{11})L_0$, $L_2 = (1+\varepsilon_{11})L_1$, etc., so that in general $L_{n+1} = (1+\varepsilon_{11})L_n$. The atomic positions are rescaled homogeneously according to the applied strain field to serve as an initial guess prior to energy minimization. The atomic coordinates change during energy minimization, approaching the equilibrium position.

After each increment of strain, we perform an energy minimization using a conjugant gradient method with a line search algorithm, carried out over $N_{\min}$ steps. We perform between $N_{\min} = 10{,}000$ (smaller protein PnIB 1AKG) and 100,000 (larger protein lysozyme 194L) minimization steps. The minimization steps are chosen conservatively to ensure convergence when the virial stress is calculated. For some cases we have confirmed that a change in magnitude of strain increments does not influence the results.

The computations are carried out within the CMDF framework, which includes Python wrappers for the NAMD code.[32,33] The computations take up to 26 hours per load increment for lysozyme 194L on a single CPU (Intel Xeon 3.06 GHz). Thus calculation of a single pressure–strain curve may take up to a weak or longer.

2.4. Calculation of Elasticity Coefficients and Stress

We calculate the pressure p after each load energy minimization, where the stresses in the protein crystal are calculated based on the virial theorem.[34,35] The pressure is given by

$$p = -\frac{1}{3}(\sigma_{11} + \sigma_{22} + \sigma_{33}) \tag{1}$$

where σ_{ij} denotes the stress tensor. We calculate the atomic stress σ_{ij} using the virial stress definition:[34]

$$\sigma_{ij} = \frac{1}{\Omega}\left(\frac{1}{2}\sum_{\alpha,\beta} -\frac{1}{r}\frac{\partial\phi}{\partial r} r_i r_{j_{r=r_{\alpha\beta}}} - \sum_{\alpha} m^{\alpha} u_i^{\alpha} u_j^{\alpha}\right) \tag{2}$$

where Ω stands for the volume of the reference cell. The virial stress of each atom is averaged over the complete unit cell, thus $\Omega = L_x L_y L_z$ (orthogonal coordinate system).

We use the NAMD molecular dynamics code that calculates the pressure according to Eqs. (1) and (2). Variations of the pressure with respect to increments in strain yields data for stress–strain curves.

2.4.1. Pressure Moduli

For uniaxial strain states imposed on the unit cell of the protein crystal, thus the strain tensor is given by

$$\varepsilon_{ij} = \begin{cases} \varepsilon & i = j = k \\ 0 & i \neq j,\ i = j \neq k \end{cases} \tag{3}$$

for uniaxial strain in the k-th direction, ε_{kk}. The stress tensor is then given by

$$\sigma_{11} = c_{11kk}\varepsilon_{kk}, \tag{4a}$$

$$\sigma_{22} = c_{22kk}\varepsilon_{kk}, \quad \text{and} \tag{4b}$$

$$\sigma_{33} = c_{33kk}\varepsilon_{kk}. \tag{4c}$$

Plugging Eqs. (4a, b, c) into Eq. (1) and taking the partial derivative with respect to ε_{kk} yields expressions related to the elastic moduli:

$$\frac{\partial p}{\partial \varepsilon_{ii}} = -\frac{1}{3}(c_{11ii} + c_{22ii} + c_{33ii}) \tag{5}$$

For example, for uniaxial strain ε_{11}, equivalent to the uniaxial strain unit cell in the x-direction:

$$\frac{\partial p}{\partial \varepsilon_{11}} = -\frac{1}{3}(c_{1111} + c_{1122} + c_{1133}) \tag{6}$$

by considering the major symmetries of the elasticity tensor. This allows the definition of three pressure moduli M_i ($i = 1.3$) that relate changes in pressure with application of uniaxial strain ε_{ii}.

The pressure moduli M_i serve as a measure for the elastic coefficients for a given loading case and are given by

$$M_1 = \frac{1}{3}(c_{1111} + c_{1122} + c_{1133}), \tag{7a}$$

$$M_2 = \frac{1}{3}(c_{1122} + c_{2222} + c_{2233}), \quad \text{and} \tag{7b}$$

$$M_3 = \frac{1}{3}(c_{1133} + c_{2233} + c_{3333}). \tag{7c}$$

The bulk modulus K is defined as

$$K = \frac{V}{\Delta V}\Delta p \tag{8}$$

where Δp is the pressure increase due to increase of the reference volume V by ΔV. This quantity is evaluated for equitriaxial strain $\varepsilon_{11} = \varepsilon_{22} = \varepsilon_{33}$. Note that

$$K = \frac{1}{3}(M_1 + M_2 + M_3) \tag{9}$$

2.4.2. Isotropic Elasticity

To obtain estimates for the elasticity coefficients and Young's modulus, we make a rough approximation and assume isotropic elasticity. Using Lamé coefficients to describe the elastic properties, and by setting $\lambda = \mu$, which is valid as long as the Cauchy-relation is satisfied so that $c_{iijj} = c_{ijij}$,[36] we arrive at

$$M = 5/3\lambda \tag{10}$$

or

$$\lambda = 3/5M \tag{11}$$

The elasticity tensor coefficients can be expressed in terms of the Lamé coefficients as $c_{1122} = c_{1212} = \lambda$ and $c_{1111} = 3\lambda$. This leads to

$$c_{1111} = 3\lambda = 9/5M \tag{12}$$

and

$$c_{1122} = \lambda = 3/5M \tag{13}$$

We consider the average of the pressure moduli in these equations, defined as

$$M = \frac{1}{3}(M_1 + M_2 + M_3) \tag{14}$$

Young's modulus is given by

$$E = 5/2\lambda = 3/2M \tag{15}$$

Bulk modulus is given by

$$K = M \tag{16}$$

Note that for such a material, $\nu = 1/4$. The obtained pressure–strain relationships are then used to calculate the tangent pressure moduli M_i, maximum stress and failure strain of the protein crystal.

We refer to those as "tangent" pressure moduli since they change with increasing strain, and we consider the local slope in the pressure–strain curves. The stress–strain curves also allow studies of plastic, non-reversible deformation of those crystals beyond the elastic instability point with zero slope.

2.5. Fracture Studies

The studies of fracture are carried out by utilizing a finite size system. Unlike for studies of elastic deformation, where only one copy of a unit cell was used, here we use a large collection of unit cells to build a macroscopic piece of material. The entire slab is strained homogeneously at each increment of loading.

2.6. Characteristic Deformation Profiles

In contrast to atomic crystals such as silicon or copper, protein crystals feature a large number of internal degrees of freedom, as the structural details at different scales constitute additional complexity and hierarchies. Local refolding, unfolding, or breaking of H-bonds within the protein may lead to regions of large deformation that appear softer than the rest of the protein, and may influence the mechanics during increase of applied strain.

We hypothesize that the response of these internal degrees of freedom plays a critical role in understanding the mechanical behavior of protein crystals.

The displacement of the backbone structure could be employed as a simple is a measure for the spatial distribution of local deformation in the protein. To investigate the response of the protein crystal to the externally applied loading at the level of deformation of each amino acid, we therefore calculate the relative displacement vector of each C_α atom in the protein crystal. Figure 4 shows a schematic introducing the concept of deformation profiles.

We define a characteristic displacement profile as

$$\Delta u^*_{i,j} = r_{C_\alpha,i} - r_{C_\alpha,j} \tag{17}$$

where $r_{C_\alpha,i}$ is the position vector of the C_α-atom at state i, and $r_{C_\alpha,j}$ that of state j. Typically the states i and j correspond to small load increments of applied strain.

The relative change in position is calculated for all C_α-atoms in the protein crystal. For N_{C_α} residues (and thus N_{C_α} C_α-atoms in the system), this leads to a matrix with dimensions $N_{C_\alpha} \times 3$. The magnitude of these displacements is useful to analyse the direction independent atomic movements, providing a measure for the overall

RESEARCH ARTICLE

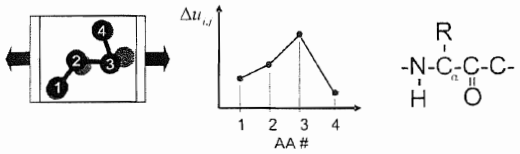

Fig. 4. Definition of the characteristic deformation profile based on the displacement of the backbone structure of the protein. This is achieved by calculating the displacement of the C_α atom within the protein crystal unit cell. The variable $\Delta u_{i,j}$ denotes the displacement of each C_α atom comparing configurations j and i. The variables j and i typically refer to increments in loading so that $j = i + 1$. The plot shows a schematic of the unit cell with and without applied load, indicating the change in locations of the C_α atoms. The variable $\Delta u_{i,j}$ represents that change. The location of the C_α atom is shown in the right of the figure. The "R" group stands for the side chain relevant for the specific amino acid considered.

atomic motion:

$$\Delta u_{i,j} = |r_{C_\alpha,i} - r_{C_\alpha,j}| \tag{18}$$

These deformation profiles provide information about the spatial distribution of deformation inside the protein crystal.

3. ELASTICITY AND FRACTURE MECHANICS OF PnIB 1AKG

First, we focus on the small protein PnIB 1AKG featuring space group P 2_1 2_1 2_1 with four proteins per unit cell. Each unit cell features approximately 1,100 atoms. The cell parameters of the orthogonal unit cell are $L_x = 14.6$ Å, $L_y = 26.1$ Å, and $L_z = 29.2$ Å. The unit cell and crystal structure are shown in Figure 5.

3.1. Elastic Properties

Figure 6 plots the pressure versus strain curve for large deformation of the protein crystal. We observe that even though for small deformation, the elastic moduli are approximately equal for uniaxial deformation in the three different orientations, there is a significant difference in the behavior for large deformation beyond 2% strain.

The breaking strain is determined by a zero slope of the pressure–strain curve that becomes negative after failure (vanishing pressure moduli).

We observe that the breaking strain is significantly different, and it is largest for the x-direction, but attains only about 78 percent of that value in the y-direction, and only about 75 percent of that in the z-direction.

We measure tangent pressure moduli $M_1 \approx 5.9$ GPa, $M_2 \approx 5.05$ GPa, and $M_3 \approx 5.08$ GPa, under small deformation. The pressure moduli decrease with increasing strain and vanish at the instability point. Considering Eq. (9), and assuming isotropic elasticity, we estimate Young's modulus to be $E \approx 8.015$ GPa. Tables I and II summarize the elastic properties for this protein crystal.

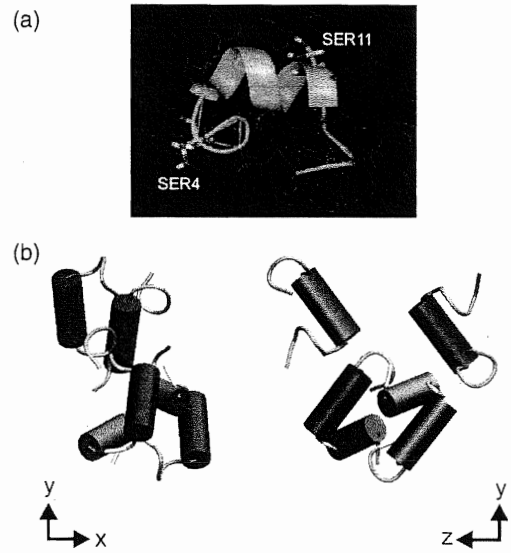

Fig. 5. Subplot (a): The protein PnIB 1AKG as crystallized and deposited in the PDB by Hu and others in 1996.[49] Subplot (b) shows two views defining the coordinate system used for our studies. We choose the same coordinate system as reported in Ref. [49].

Breaking of the protein crystal at the theoretical strength is characterized by the instability at a zero slope in the stress–strain plot.

From studies with equitriaxial loading, we estimate the bulk modulus of PnIB 1AKG as $K \approx 4.69$ GPa. From Eq. (9), bulk modulus $K \approx 5.34$ GPa. The slight deviation may suggest that deformation is path dependent, possibly indicating some permanent deformation mechanisms even for small strains.

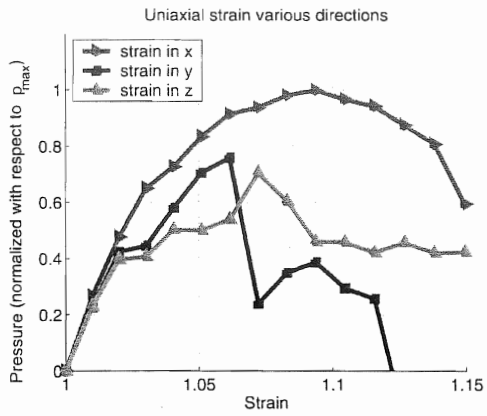

Fig. 6. Elastic and plastic response of a perfect crystal of PnIB 1AKG.[49] The perfect crystal shows strong nonlinear behavior with strong softening at large strain. The crystal breaks at large strain (negative tangent slope). The results are shown for loading in three different directions, suggesting a strong impact of crystallographic orientation on the mechanical properties.

Table I. Summary of mechanical properties of the two wild type protein crystals studied in this paper.

Protein crystal	M_1 (GPa)	M_2 (GPa)	M_3 (GPa)	M (GPa)	K (GPa)
PnIB 1AKG	5.90	5.05	5.08	5.34	4.69
Lysozyme 194L	0.626	0.701	0.561	0.629	0.22

Table II. Summary of mechanical properties of various protein crystals studied in this paper. The results are obtained by assuming isotropic linear elasticity as discussed in Section 2.4.2.

Protein crystal	Young's modulus E (GPa)	Shear (GPa) modulus $\mu = c_{1212} = c_{1122}$	Elasticity coefficient c_{1111} (GPa)
PnIB 1AKG	8.015	3.204	9.612
Lysozyme 194L	0.944	0.377	1.132

3.2. Effect of Mutations on Elastic Properties

Now we study the effect of mutations in the amino acid sequence on the overall mechanical behavior. We focus on the effect of replacing two polar, neutral amino acid residues SER4 and SER11 (locations are indicated in Fig. 5(a)).

The original protein is referred to as case 0 (wild type). We replace these two residues by non-polar, neutral residues (mutation SER→ALA or S4A S11A; referred to as case 1), as well as by polar, acidic non-neutral residues (mutation SER→ASP or S4D S11D; referred to as case 2).

Figure 7 depicts the stress versus strain relationship for these three cases, for loading in the x-direction. We observe a significant effect of these mutations on the elastic properties.

In case 1 (S4A S11A), we see a significant reduction in both breaking strain (to 78% of the original value) as well as maximum stress (to 70% of the original value). In case 2 (S4D S11D), we find a significant increase of the breaking strain (to 120% of the original value) and the maximum stress (to 124% of the original value).

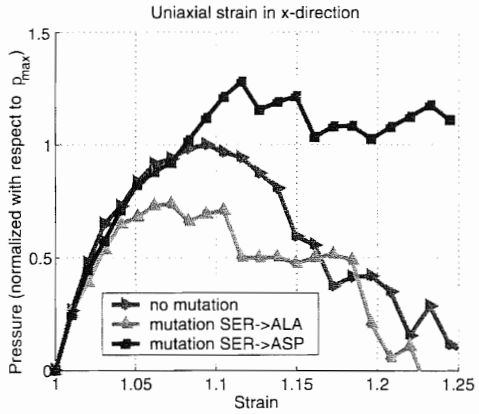

Fig. 7. The effect of dual point mutations on the overall macroscopic response of the protein crystal of PnIB 1AKG. The mutation SER→ALA (S4A S11A) leads to a decrease of strength and maximum pressure, whereas the mutation SER→ASP (S4D S11D) has the reverse effect and makes the crystal stronger. The plot shows pressure versus strain curves (curves normalized by the maximum pressure of the original protein).

These observations may be explained by the fact that the SER→ASP mutation leads to increased ionic interactions in the crystal thus making the material stronger. In contrast, introducing the non-polar and neutral residue SER→ALA leads to reduced ionic interactions and thus a less strong material behavior. These results indicate the potentially large impact of even small changes of the amino acid sequence on the mechanics of protein crystals.

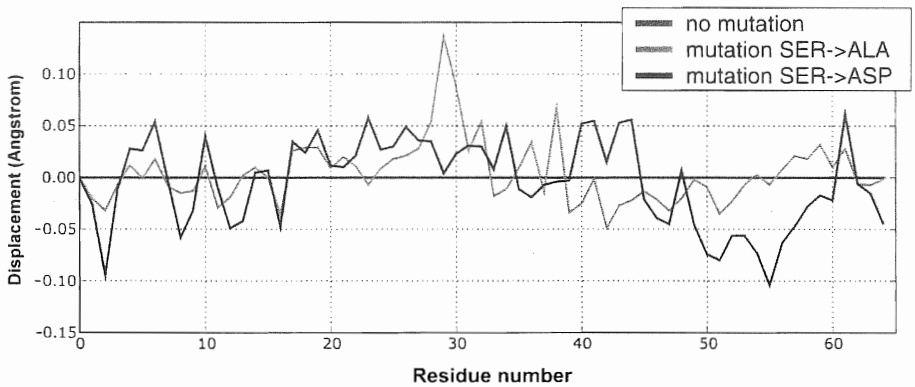

Fig. 8. Comparison of deformation profiles of non-mutated and mutated PnIB 1AKG, showing the difference between the unmated and mutated cases, defined as $\Delta u_{i,j}^{\text{diff}} = \Delta u_{i,j}^{\text{mut}} - \Delta u_{i,j}^{\text{nomut}}$. In all cases, we consider a deformation state three loading steps from breaking, thus we are in the large-strain regime where the mechanics is significantly different (for no mutation, $(j,i) = (7,6)$, for SER→ALA (S4A S11A) $(j,i) = (4,3)$ and for SER→ASP (S4D S11D) $(j,i) = (9,8)$, thus the applied strain is different in all three cases). We notice a difference in the profiles, for each mutation. For the mutation SER→ALA (S4A S11A), we see one hotspot of large deformation at residue 29, probably leading to local large stresses thus relatively low strength. The mutation SER→ASP (S4D S11D) shows a different, but more even profile, with regions where the displacement is reduced (for example, in residues 48–60), probably due to stronger interactions.

It also suggests that electrostatic interactions could play a critical role.

3.3. Effect of Mutations on Microscopic Displacements: Characteristic Displacement Profiles

The characteristic displacements defined in Section 2.6 provide information about how the mutations influence the microscopic changes in displacements.

Figure 8 shows a comparison of deformation profiles of non-mutated and mutated PnIB 1AKG by plotting

$$\Delta u^{\text{diff}} = \Delta u^{\text{mut}}_{i,j} - \Delta u^{\text{no mut}}_{k,l} \tag{19}$$

In all cases, we consider a deformation state three loading steps (ca. 0.03% strain) from breaking. This corresponds to the large-strain regime where the mechanical response of the mutated protein crystals is significantly different (Fig. 7).

For the mutation SER→ALA (S4A S11A), we see one hotspot of large deformation at residue 29, probably leading to local large stresses thus relatively low strength.

The mutation SER→ASP (S4D S11D) shows a different profile that appears to show more evenly distributed displacements, with regions where the displacement is reduced. This can be confirmed in residues 48–60, for example. These observations are not inconsistent with the notion that the mutation of SER to ASP leads to stronger interactions, making the crystal stronger.

3.4. Surface Energies

The surface energies are calculated by comparing the energies of a unit cell with a free surface and without a free surface, by normalizing with respect to the surface area. The protein structure is relaxed using an energy minimization scheme in both cases.

For fracture analyses, it is essential to calculate the fracture surface energies. Based on atomistic simulation, we have determined the surface energies for different crystallographic orientations. For the (010) surface, $\gamma = 0.205$ N/m, for the (100) surface, $\gamma = 0.257$ N/m, and for the (001) surface, we find that $\gamma = 0.343$ N/m.

We note that the presence of water will likely significantly change the surface energies of the protein crystals. This is not considered in this study.

3.5. Fracture Behavior Under Mode I Tensile Loading

Modeling the dynamics of fracture of materials with atomistic simulation has become a widely accepted and extremely fruitful approach in the materials community (see, for example Refs. [37–42] describing studies of brittle fracture). However, to the best of our knowledge such techniques have not been applied to model fracture of protein crystals.

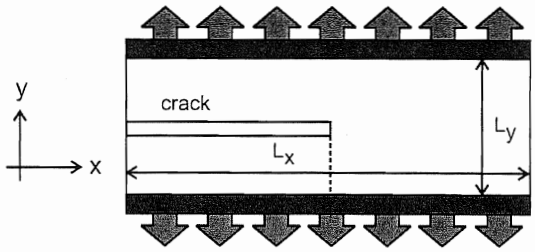

Fig. 9. Geometry used for the fracture studies of protein crystals. We start with a large crystal of PnIB 1AKG,[49] with a small slit serving as initial defect for nucleation of the crack. The slit is implemented by taking out a row of proteins in the protein crystal, thus creating the crack-like defect. We then gradually increase the strain applied to the system according to mode I (tensile) loading. We use periodic boundary conditions in the x- and z (out-of-plane) direction.

For studies of dynamic fracture of protein crystals, we start with a large crystal of PnIB 1AKG, with a small slit serving as the initial defect for nucleation of the crack.

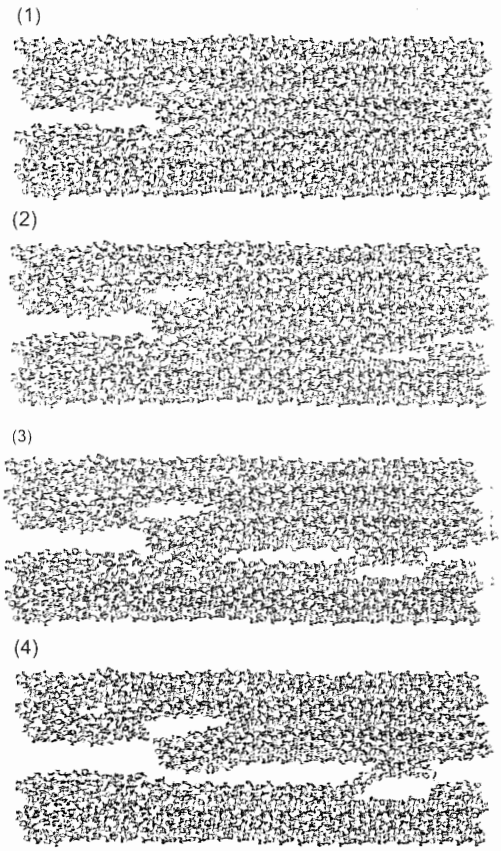

Fig. 10. Snapshots of the dynamics of fracture of a protein crystal of PnIB 1AKG.[49] After a critical load is reached, the crack starts to nucleate. Note that periodic boundary conditions are applied in the x-direction so the crack starts to nucleate at both sides (geometry of the simulation see Fig. 5). This system contains about 130,000 atoms.

RESEARCH ARTICLE

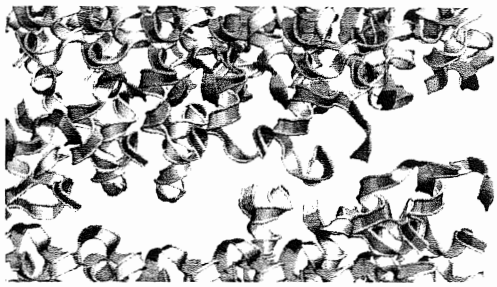

Fig. 11. Crack propagation creates a round fracture surface due to local refolding of the protein during crack motion. Observation of such detail in fracture behavior is only possible using atomistic simulation. Bonds within a protein do not break, only bonds between different protein molecules that are columbic, H-bonds or dispersive vdW interactions.

The slit is generated by taking out one row of proteins. We use $24 \times 5 \times 1$ unit cells for this finite system, leading to a size $L_x = 350.4$ Å, $L_y = 130.5$ Å, and $L_z = 29.2$ Å. We assume periodic boundary conditions in all three directions, so the crack corresponds to a penny-shaped configuration. The geometry of the fracture studies is schematically shown in Figure 9.

We gradually increase the applied strain applied to the system according to mode I (tensile) loading. The fracture surface is chosen to be (010) (due to lowest fracture surface energy along this direction, see discussion above).

Figure 10 depicts snapshots of crack dynamics in the protein crystal. We observe that multiple small cracks nucleate at the critical load.

Crack propagation creates a circular shaped fracture surface due to local refolding of the protein during crack motion, as can be verified in Figure 11. Such insight into materials deformation mechanisms is only possible with atomistic level calculations.

4. ELASTICITY OF LYSOZYME (PDB ID 194L)

Here we discuss small and large-strain elasticity and plasticity of crystals of lysozyme (PDB ID 194L). We consider the 1.4 Å structure of tetragonal hen egg white lysozyme as crystallized during the spacehab-01 mission, and analyzed by Vaney and coworkers[43] in X-ray diffraction experiments.

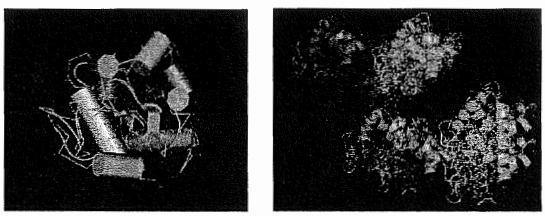

Fig. 12. Cartoon drawing of the protein (single protein, left) and the unit cell of the protein with eight molecules (right).

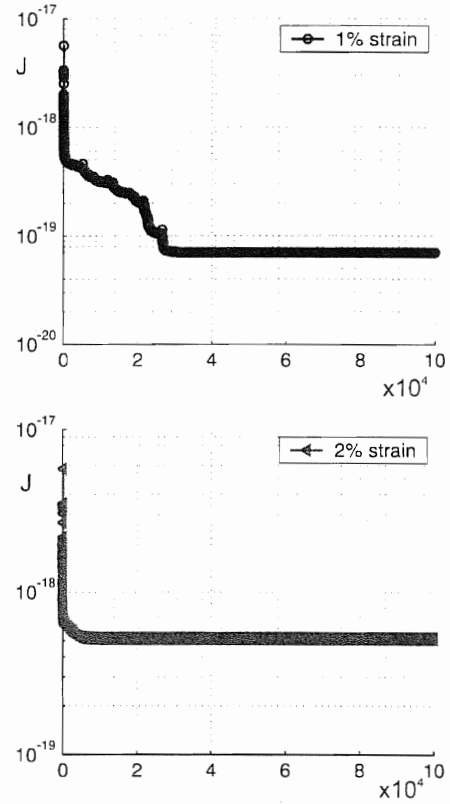

Fig. 13. Confirmation of convergence of the energy minimization calculations. The log–log plots show the potential energy as a function of iteration steps (the two graphs show the results for two increments of applied strain in discrete steps of 1% each). We carry out 100,000 iterations of minimization after each application of strain increment. As can be verified by the plots, the energy converges after each application of load increment.

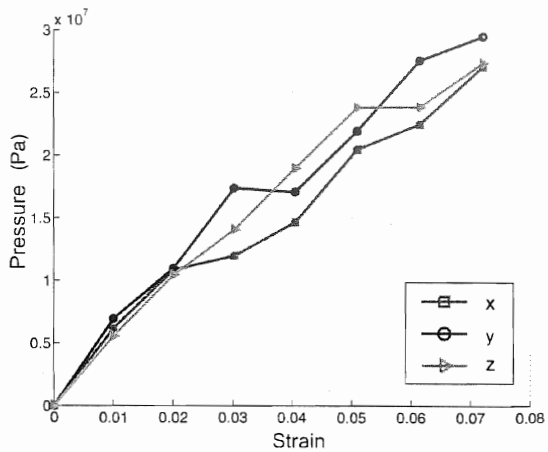

Fig. 14. Pressure versus strain for uniaxial strain applied in the x, y, and z-direction direction, with no poisson relaxation applied in the lateral direction (protein lysozyme 194L).

RESEARCH ARTICLE

4.1. Structural Details of Lysozyme and Computational Procedure

Lysozyme has 129 residues with four disulfide cross-links within each protein molecule. Several salt bridges (i.e., ionic interactions between oppositely charged residues) exist between proteins in the crystal and within each protein. This crystal structure is represented by the space group P 4_3 2_1 2 and forms tetragonal crystals with 8 proteins per unit cell (1,032 total residues and approximately 18,000 atoms per unit cell). Compared with the protein studied in Section 3, lysozyme 194L has much more residues and a more complex three-dimensional fold.

The crystal features eight proteins per unit cell. We plot the structure of a single lysozyme protein and the crystal unit cell in Figure 12. The cell parameters of the orthogonal unit cell are $L_x = L_y = 78.65$ Å and $L_z = 37.76$ Å.

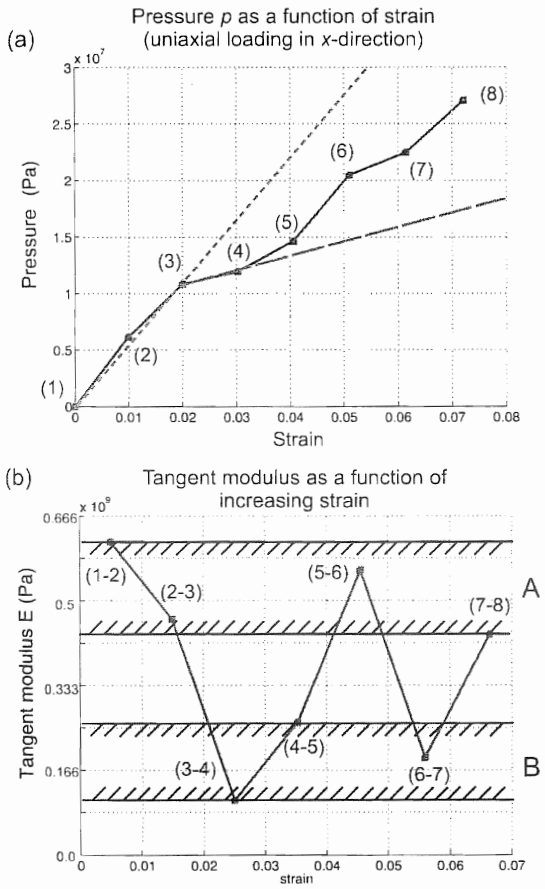

Fig. 15. Subplot (a): Pressure versus strain for uniaxial strain applied in the x-direction, no Poisson relaxation in lateral direction (protein lysozyme 194L). Subplot (b): Tangent pressure modulus as a function of increasing strain. We note that the results for the tangent pressure moduli fall into two windows (regimes "A" and "B"). We have also confirmed that the pressure–strain behavior is independent of increments of load (results not shown).

Before simulations are started and strain is applied, the energy of the initial structure is relaxed at no load applied. Figure 13 depicts the potential energy as a function of iteration steps, clearly showing that convergence is reached when the minimization is stopped.

We carry out 100,000 iterations of minimization after each strain increment application. As can be seen in the plots, the energy converges after each application of load increment. The resulting structure of previous energy minimization runs is used as the input structure when additional strain is applied. This procedure is applied repeatedly as the strain is increased.

As in the earlier studies, we apply uniaxial strain ε_{ii}, where $i = 1, 2, 3$, without relaxation in the lateral directions. This procedure is identical to the studies of PnIB 1AKG.

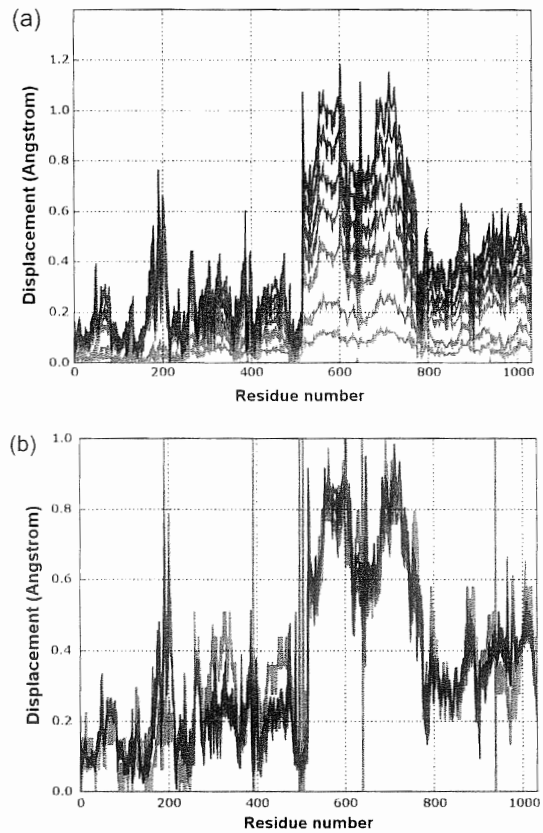

Fig. 16. Characteristic deformation profiles for the C_α atom (relative to the previous loading step), while the strain is increased slowly in strain increments 0.25% (green = 0% strain, red = 1.76% strain). The protein crystal shows linear elasticity in this regime (see Fig. 15(a)). Subplot (a) shows the original data, indicating the characteristic displacements increase as the strain is increased. Subplot (b) shows the same data normalized with respect to the maximum displacement for a given load increment. We observe that all curves fall close to one master curve, suggesting that the displacement profile represents a certain elasticity of the protein crystal.

4.2. Elastic Properties of Lysozyme

Figure 14 plots pressure versus strain for three different directions of uniaxial strain, where loading is applied in the x, y, and z-direction. We measure tangent pressure moduli of $M_1 \approx 0.626$ GPa, $M_2 \approx 0.701$ GPa, and $M_3 \approx 0.561$ GPa. These pressure moduli are evaluated at small strains. These results suggest a slight orientation dependence of elasticity. Our simulations indicate that the bulk modulus is $M = K \approx 0.22$ GPa. As an alternative, the average of the three pressure moduli in Eq. (9) can be used to determine an estimate for the bulk modulus, which is $M = 1/3(M_1 + M_2 + M_3) \approx 0.629$ GPa.

We estimate $c_{1111} \approx 1.88$ GPa, $c_{1122} \approx 0.629$ GPa. Young's modulus is $E \approx 0.943$ GPa, and the shear modulus is $\mu \approx 0.629$ GPa. Tables I and II summarize the elastic properties for this protein crystal.

Speziale and coworkers[7] obtained values for $c_{1111} \approx 5.49$ GPa and $c_{3333} \approx 5.48$ GPa by Brillouin scattering experiments in tetragonal crystals of hen egg white lysozyme. The numerical values of the elastic constants are about one order of magnitude different from experimental results. Similarly, the bulk modulus obtained by MD simulation is much smaller than the result of experimental measurements, featuring values between 2 and 5 GPa.

4.3. Characteristic Deformation Profiles of Lysozyme 194L

Here we focus on loading in the x-direction and analyze the internal deformation mechanisms. Figure 15 depicts the pressure as a function of uniaxial loading in the x-direction (subplot (a)), including the tangential pressure moduli (subplot (b)).

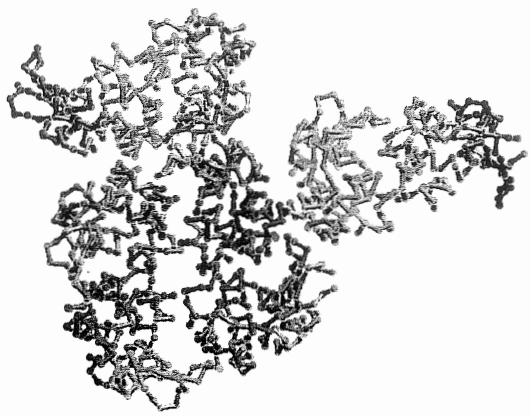

Fig. 17. Relative displacement of C_α atoms during deformation, showing a three-dimensional "mesoscopic" view of a single unit cell of lysozyme 194L (we compare 0% strain with 1.76% uniaxial strain). The results confirm deformation is not homogeneous, with specific hotspots of deformation indicated by the red color (blue color denotes small or no deformation). We further find that some domains participate strongly in deformation, while others less.

Figure 16 plots the characteristic deformation profiles as defined in Eq. (18), up to strains of around 1.76%. The plot depicts the change of the displacement relative to the previous loading step. Subplot (a) shows the original data, indicating that the displacements increase as the strain is increased. Subplot (b) shows the same data normalized with respect to the maximum displacement in each profile. All curves fall together to one master curve. Figure 17 shows a 3D view of the magnitude of displacements, clearly showing the hotspots of deformation in the unit cell.

Figure 18 depicts the characteristic displacement profiles for larger strains. Subplot (a) shows all residues, where as subplot (b) shows a zoom into residues 400 to 800. Subplot 19 depicts all profiles that correspond to the same tangent pressure modulus in Figure 15. We observe

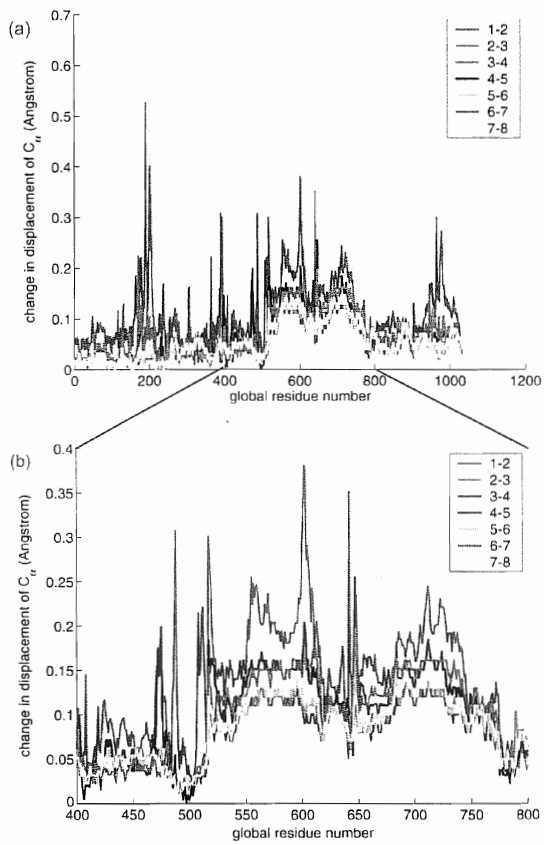

Fig. 18. Characteristic deformation profiles for the C_α atoms (displacements relative to the previous loading step, strain increments of 1%). Subplot (a) shows the characteristic profiles for all residues. Subplot (b) depicts the characteristic deformation profile for residue numbers 400 to 800, allowing a closer look at the individual curves. We observe certain regions with extremely large deformation that may initiate failure or change in deformation mode (e.g., (1–3) around residue #610).

RESEARCH ARTICLE

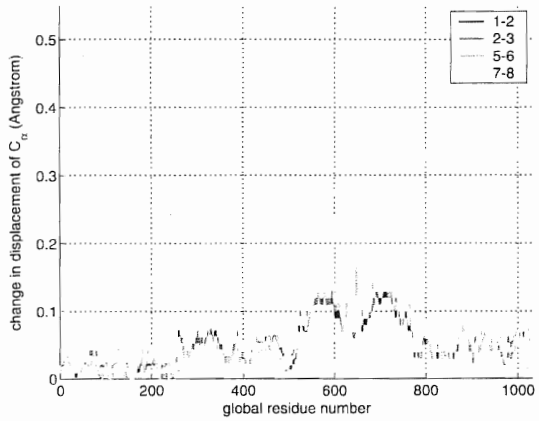

Fig. 19. Characteristic deformation profiles for the C_α atoms (displacements relative to the previous loading step, strain increments of 1%). This plot shows the profiles for load increments 1–2, 2–3, 5–6, and 7–8. All profiles fall on one curve, and all those load increments show the same tangential modulus (see Fig. 14(b), regime "A").

that some of the deformation profiles are grouped together, and all data points fall onto a single curve.

These results are indicative of the fact that the internal degrees of freedom can be linked to the overall macroscopic mechanical response.

The results shown in Figures 16(a) and (b) suggest that the magnitude of the deformation profile is proportional to the applied strain, or

$$\Delta u_{i,j} \sim \Delta \varepsilon^{i \to j} \tag{20}$$

Further, the results shown in Figures 18 and 19 indicate that the characteristic deformation profiles can be linked with local or tangential elasticity ($M_{i,j}$ describes the tangent pressure modulus for load increments from state i to j).

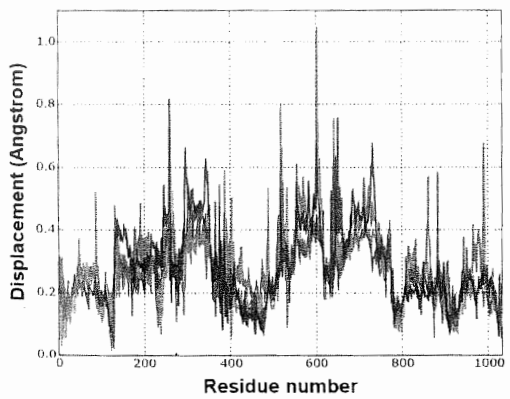

Fig. 20. Characteristic deformation profiles for the C_α atoms (displacements relative to the previous loading step, showing four strain increments of approximately 0.5% each, for equitriaxial loading. All profiles fall on one curve, and all those load increments show a similar tangential bulk modulus.

There seems to be a correspondence between the deformation profile and tangent pressure moduli $M_{i,j}$:

$$M_{i,j} = \tilde{f}_M(\Delta u_{i,j}) \tag{21}$$

where $\tilde{f}_M$ is an unknown function. Eqs. (20) and (21) may provide important information about the origin of elasticity in protein crystals.

We have also evaluated the displacement profile for equitriaxial loading, and observed a similar behavior as for the uniaxial loading cases. As before, deformation is inhomogeneous inside the protein crystal. Figure 20 shows four characteristic displacement profiles up to 2% strain, with increments of 0.5% each. Even though the overall deformation is equal in all three directions, the internal relaxation mechanisms show inhomogeneous behavior.

5. DISCUSSION AND CONCLUSION

We have reported atomistic modeling to calculate the elastic properties of protein crystals using the empirical AMBER[29] force field.

- We have shown that mutations in primary sequence influence macroscopic elasticity: Double point mutations can lead to both reduction and increase of maximum stress and failure strain, indicating a potential in tuning mechanical properties of protein-based material by sequence changes (see the results shown in Fig. 7). The significance of such effects to understand biological processes and for new materials development remains to be explored.
- The new concept of characteristic deformation profiles defined in Section 2.6 constitute a useful measure to characterize the response of internal degrees of freedom of protein crystals due to mechanical stimulation. This or similar methods may be applied to characterize the mechanical response of other biological materials.
- We have shown that amino acid sequence changes have some impact on the deformation profiles. Figure 8 showed that the mutation SER→ALA induces strong deformation localization, possibly explaining the reduced strength. Similarly, the mutation SER→ASP reduced the amount of deformation, even in the large strain regime, thus making the protein crystal stronger. Such studies help to improve our understanding of cross-scale interactions as introduced in Figure 2, linking molecular or microstructural deformation patterns with the overall elastic response.
- We have discovered that specific patterns in the displacement of the C_α-atoms can be linked to local, tangent pressure moduli during deformation (see discussion in Section 4.3). We could associate changes in local elasticity with characteristic deformation profile shapes; whenever a similar slope in the pressure–strain curve is observed, the deformation profile falls onto the same curve.
- The magnitude of the deformation profiles is proportional to the magnitude of the applied strain increment (see discussion in Section 4.3 and Fig. 16).

RESEARCH ARTICLE

- We have shown that even for equitriaxial or hydrostatic strain loading, deformation within the unit cell of the protein crystal is inhomogeneous (see Fig. 20).
- Calculation of the bulk modulus K of lysozyme 194L allowed comparison with experimental predictions, indicating that our model significantly underestimates the quantitative values obtained by experimental results. We also include a prediction for the bulk modulus of PnIB 1AKG. We find that the smaller protein PnIB 1AKG is elastically much stiffer than lysozyme 194L (ratio of bulk moduli $K_{1AKG}/K_{194L} \approx 21.31$).

Experimental studies are critical to confirm the predictions made by our studies focusing on the effect of mutations. Such investigations may already be possible with the experimental techniques available today. Similar techniques as reported here could be used to perform systematic optimization and tailoring of the elastic properties of protein crystals, combining theory, and experiment.

Elastic deformation of protein crystals is characterized by small displacements of the atoms in the three-dimensional folded structure. Plastic deformation includes refolding of the protein into a new three-dimensional folded structure. This unfolding may occur locally and involve only certain domains of the protein. These mechanisms are not inconsistent with our observations of deformation hotspots, as for example shown in Figure 17.

In preliminary studies of fracture of protein crystals, we have demonstrated that atomistic modeling of cracking of chemically complex biological materials using large-scale molecular dynamics simulations is feasible. Atomistic modeling can be a valuable "computational microscope" to understand the deformation of protein crystals. We leave models of larger systems with different crack orientations, and comparison with Griffith's theories of fracture to future investigations.

Our results suggest that methods such as the Cauchy-Born (C-B)[44,45] rule cannot be applied to complex biological materials such as protein crystals, because of the significant internal relaxations: The macroscopic continuum deformation field can not be imposed on the atomic coordinates. However, once mapping functions for the backbone atoms are determined (for example, based on characteristic deformation profiles), new numerical schemes could be developed that take these displacements into consideration. The folded structure of proteins constitutes a layer of complexity that defines the response of the material to mechanical stimulation by the interplay of various types of chemical bonds.

Future studies could be focused on using more accurate force fields for modeling deformation, including the possibility for bond breaking and formation.[23] Further, it may be interesting to extend the studies to relate the response of distinct domains of the protein during deformation to their biological function.

This may also be used to advance our understanding of diseases and potentially lead to development of new drugs. For example, a study as described here could be carried out to analyze the mechanics of protein crystals that form in sickle cell amenia, or in Alzheimer's disease where amyloid beta peptides form amyloid plaques. Modifications of the mechanical stability, adhesion properties or chemical reactivity of these protein crystals due to solvent effects, mutations or variations in the boundary conditions may help to contribute to advance the molecular origins of the these diseases.

Specific engineering of the material behavior based on this knowledge may be beneficial to design new materials. Additional studies could be focused on the effect of water content in the protein crystal on the mechanical properties.[46,47] Experiment suggests a strong impact of water concentration on the mechanical properties.

Further, loading–unloading calculations will be helpful to determine the existence and degree of plastic deformation in the samples. This may also help to explain the deviation of estimates of the bulk modulus from hydrostatic and uniaxial loading. The analysis of elastic coefficients reported in this paper has been carried out under the assumption of isotropic material behavior. Future studies could focus on analyzing the individual stress tensor contributions to investigate the effect of anisotropy and to estimate the elastic coefficients for different crystallographic directions.

Acknowledgments: M. J. B. acknowledges generous support from MIT's CEE Department. Most of the calculations and the analysis were carried out using a LINUX computer at MIT's Atomistic Mechanics Modeling Laboratory.

References

1. D. X. Cui and H. J. Gao, *Biotechnology Progress* 19, 683 **(2003)**.
2. M. Knoblauch and W. S. Peters, *Cell. Mol. Life Sci.* 61, 2497 **(2004)**.
3. H. Gao, Y. Kong, D. Cui, and C. S. Ozkan, *Nano Lett.* 3, 471 **(2003)**.
4. F. H. Wilt, *Developmental Biology* 280, 15 **(2005)**.
5. H. Gao, B. Ji, I. L. Jäger, E. Arzt, and P. Fratzl, *Proc. Natl. Acad. Sci. USA* 100, 5597 **(2003)**.
6. C. Sanchez, B. Julian, P. Belleville, and M. Popall, *J. Mater. Chem.* 15, 3559 **(2005)**.
7. G. S. Sayler, M. L. Simpson, and C. D. Cox, *Curr. Opin. Microbiol.* 7, 267 **(2004)**.
8. C. Montemagno and G. Bachand, *Nanotechnology* 10, 225 **(1999)**.
9. R. Spolenak, S. Gorb, and E. Arzt, *Acta Biomaterialia* 1, 5 **(2005)**.
10. H. J. Gao, X. Wang, H. M. Yao, S. Gorb, and E. Arzt, *Mech. Mater.* 37, 275 **(2005)**.
11. M. S. Gudiksen, L. J. Lauhon, J. Wang, D. C. Smith, and C. M. Lieber, *Nature* 415, 617 **(2002)**.
12. S. A. Maskarinec and D. A. Tirrell, *Curr. Opin. Biotechnol.* 16, 422 **(2005)**.
13. R. Langer and D. A. Tirrell, *Nature* 428, 487 **(2004)**.
14. W. A. Petka, J. L. Harden, K. P. McGrath, D. Wirtz, and D. A. Tirrell, *Science* 281, 389 **(1998)**.

15. J. M. Smeenk, M. B. J. Otten, J. Thies, D. A. Tirrell, H. G. Stunnenberg, and J. C. M. van Hest, Controlled Assembly of Macromolecular Beta-Sheet Fibrils, Angewandte Chemie-International Edition (**2005**), Vol. 44, pp. 1968–1971.
16. G. M. Whitesides and A. P. Wong, *MRS Bull.* 31, 19 (**2006**).
17. S. Suresh, J. Spatz, J. P. Mills, A. Micoulet, M. Dao, C. T. Lim, M. Beil, and T. Seufferlein, *Acta Biomater.* 1, 15 (**2005**).
18. G. Bao and S. Suresh, *Nat. Mater.* 2, 715 (**2003**).
19. O. de Carmejane, M. D. Morris, M. K. Davis, L. Stixrude, M. Tecklenburg, R. M. Rajachar, and D. H. Kohn, *Calcified Tissue International* 76, 207 (**2005**).
20. O. Galkin, K. Chen, R. L. Nagel, R. E. Hirsch, and P. G. Vekilov, *Proceedings of the National Academy of Sciences of the United States of America* 99, 8479 (**2002**).
21. M. Springborg, Density-functional methods in chemistry and materials science. Wiley Research Series in Theoretical Chemistry (**1997**).
22. A. D. Becke, *J. Chem. Phys.* 98, 5648 (**1993**).
23. A. C. T. v. Duin, S. Dasgupta, F. Lorant, and W. A. Goddard, *J. Phys. Chem. A* 105, 9396 (**2001**).
24. E. Villa, A. Balaeff, L. Mahadevan, and K. Schulten, *Multiscale Modeling and Simulation* 2, 527 (**2004**).
25. A. C. Lorenzo and E. R. Caffarena, *J. Biomech.* 38, 1527 (**2005**).
26. K. Hinsen, *J. Comput. Chem.* 21, 79 (**2000**).
27. A. D. MacKerell, D. Bashford, M. Bellott, R. L. Dunbrack, J. D. Evanseck, M. J. Field, S. Fischer, J. Gao, H. Guo, S. Ha, D. Joseph-McCarthy, L. Kuchnir, K. Kuczera, F. T. K. Lau, C. Mattos, S. Michnick, T. Ngo, D. T. Nguyen, B. Prodhom, W. E. Reiher, B. Roux, M. Schlenkrich, J. C. Smith, R. Stote, J. Straub, M. Watanabe, J. Wiorkiewicz-Kuczera, D. Yin, and M. Karplus, *J. Phys. Chem. B* 102, 3586 (**1998**).
28. M. T. Nelson, W. Humphrey, A. Gursoy, A. Dalke, L. V. Kale, R. D. Skeel, and K. Schulten, *International Journal of Supercomputer Applications and High Performance Computing* 10, 251 (**1996**).
29. D. A. Pearlman, D. A. Case, J. W. Caldwell, W. S. Ross, T. E. Cheatham, S. Debolt, D. Ferguson, G. Seibel, and P. Kollman, *Comput. Phys. Commun.* 91, 1 (**1995**).
30. B. R. Brooks, R. E. Bruccoleri, B. D. Olafson, D. J. States, S. Swaminathan, and M. Karplus, *J. Comput. Chem.* 4, 187 (**1983**).
31. M. P. Allen and D. J. Tildesley, Computer Simulation of Liquids, Oxford University Press (**1989**).
32. M. J. Buehler, J. Dodson, P. Meulbroek, A. Duin, and W. A. Goddard, *Mater. Res. Soc. Proc.* 894, LL3.8 (**2006**).
33. M. J. Buehler, A. C. T. v. Duin, and W. A. Goddard, *Phys. Rev. Lett.* 96, 095505 (**2006**).
34. D. H. Tsai, *J. Chem. Phys.* 70, 1375 (**1979**).
35. M. Zhou, *Phil. Mag. A* 82 (**2002**).
36. M. I. Baskes, *Phys. Rev. B* 29, 6443 (**1984**).
37. B. deCelis, A. S. Argon, and S. Yip, *J. Appl. Phys.* 54, 4864 (**1983**).
38. K. S. Cheung and S. Yip, *Model. Simul. Mater. Eng.* 2, 865 (**1993**).
39. M. J. Buehler, F. F. Abraham, and H. Gao, *Nature* 426, 141 (**2003**).
40. F. F. Abraham, D. Brodbeck, W. E. Rudge, and X. Xu, *J. Mech. Phys. Solids* 45, 1595 (**1997**).
41. F. F. Abraham, D. Brodbeck, R. A. Rafey, and W. E. Rudge, *Phys. Rev. Lett.* 73, 272 (**1994**).
42. M. J. Buehler and H. Gao, *Nature* 439, 307 (**2006**).
43. M. C. Vaney, S. Maignan, M. RiesKautt, and A. Ducruix, *Acta Crystallographica Section D-Biological Crystallography* 52, 505 (**1996**).
44. J. J. Weiner, *Phys. Rev. B* 24, 845 (**1983**).
45. M. Born and K. Huang, Dynamical Theories of Crystal Lattices. Clarendon, Oxford (**1956**).
46. C. L. Caylor, S. Speziale, S. Kriminski, T. Duffy, C. S. Zha, and R. E. Thorne, *J. Cryst. Growth* 232, 498 (**2001**).
47. S. Speziale, F. Jiang, C. L. Caylor, S. Kriminski, C. S. Zha, R. E. Thorne, and T. S. Duffy, *Biophys. J.* 85, 3202 (**2003**).
48. T. Michon and D. A. Tirrell, *Biofutur* 2000, 34 (**2000**).
49. S. H. Hu, J. Gehrmann, L. W. Guddat, P. F. Alewood, D. Craik, and J. L. Martin, *Structure* 4, 417 (**1996**).

Received: 3 March 2006. Accepted: 1 April 2006.

RESEARCH ARTICLE